The effect of water on strain localization in calcite fault gouge sheared at seismic slip rates

By Tyler Lagasse

Introduction

- Co-seismic slip depth limited within sub-cm-thick gouge & cataclastic-bearing principal slip zones

- Localization to sub-mm scale during single co-seismic slip events

- High-velocity (V_{max} = 1 m/s) rotary-shear experiments @ normal stress (σ_n) of 3-20 Mpa done under room-dry & wet conditions

- Natural fault zones in limestone more susceptible to rapid dynamic weakening if water is in granular slipping zones

Material & methods

- There were 2 different rotary-shear apparatus utilized
  - I. Slow to High Velocity Apparatus (SHIVA)
  - II. Pressurized High-Velocity (Phv)

Setup of SHIVA

- 18 experiments using strain markers
- Max. slip rate: 1 m/s
- Accel. & Decel.: 6 m/s^2
- σ_n: 3-20 Mpa
- Total displacements: 0.011-2.5 m under room-dry & water-dampened condiditons
- Gouge layer inner/outer diameters: 35 & 55 mm

Table 1
Experiments performed with SHIVA. Experimental conditions applied in the a) room-dry and b) water-dampened strain-marker experiments. Equivalent target slip rate was 1 m/s in all experiments.

	Experiment	Normal stress (MPa)	Total equivalent displacement (m)	Applied bulk strain[a]	Max. bulk strain rate (1/s)[a]	Thickness (mm)[c]	Initial thickness (mm)[e]
a) Room-dry	s897	3	0.29	128	441	2.14	2.27
	s886	3	2.5	1295	518	1.8	1.93
	s873	8.5	0.08	32	400	–	–
	s953	8.5	0.13	60	463	1.41	2.16[d]
	s871	8.5	0.28	112	400	–	–
	s887	8.5	0.29	109	376	2.5	2.66
	s881	8.5	0.43	195	452	2.02	2.21
	s1013	8.5	0.43	172	400	–	–
	s952	8.5	0.5	200	400	–	–
	s896	8.5	1.3	442	340	2.6	2.94
	s943	8.5	1.3	551	424	2.1	2.36
	s875	15	0.14	56	400	–	–[d]
	s889	20	0.29	141	488	1.93	2.05[d]
b) Water-dampened[b]	s959	8.5	0.011	6	230	1.64	1.74
	s895	8.5	0.2	80	400	–	0.9[d]
	s961	8.5	0.43	228	529	1.74	1.89
	s898	8.5	1.5	732	488	1.9	2.05
	s962	8.5	2.1	1148	546	1.55	1.83
	s279[f]	17.3	2.82	1128	400	–	–
	s389[f]	21	1.015	406	400	–	–

[a] If no initial sample thickness could be calculated, a thickness of 2.5 mm was assumed.
[b] 20 wt% distilled H_2O.
[c] Thickness of sheared gouge layer evaluated from the SEM pictures.
[d] Material loss during sample preservation.
[e] Obtained from [c] and the amount of compaction measured during the experiment.
[f] No strain marker.

Setup of Phv

- 24 experiments under room-dry & controlled pore-pressure conditions

- Max. slip rate:1 m/s

- Acceleration: 0.5 m/s^2

- Gouge layer inner/outer diameters: 30 & 60 mm

- σ_n: 3-12 Mpa

- Pore-fluid pressure: 0.2-1.5 Mpa

- Perfomed w/room-dry & water-saturated conditions, no strain markers

- Data recorded @ 1 kHz rate

Table 2
Experiments performed with the Phv apparatus. Experimental conditions applied in the a) room-dry and b) water-saturated experiments. Equivalent target slip rate was 1 m/s in all experiments.

	Experiment	Normal stress (MPa)	Fluid pressure (MPa)	Total equivalent displacement (m)	Pre-sheared?
a) Room-dry	phv311	3	—	5.5	Y
	phv343	3	—	3.72	N
	phv299	8.5	—	15.62	Y
	phv301	8.5	—	17.62	Y
b) Water-saturated	phv305	1	1.5	18.42	Y
	phv306	1	0.2	19.22	Y
	phv290	3	7	22.00	Y
	phv304	3	1.5	19.12	Y
	phv310	3	0.6	5.31	Y
	phv313	3	0.6	5.32	N
	phv337	3	7	4.86	Y
	phv347	3	7	3.88	N
	phv355	3	7	2.18	Y
	phv340	4	6	4.92	Y
	phv351	4.5	10.5	4.03	Y
	phv350	6	9	4.25	Y
	phv291	8.5	1.5	22.70	Y
	phv292	8.5	1.5	16.06	Y
	phv297	8.5	1.5	18.40	Y
	phv298	8.5	1.5	17.43	Y
	phv300	8.5	1.5	9.91	Y
	phv312	8.5	1.5	5.12	Y
	phv307	10	2	4.82	Y
	phv309	12	1.5	12.82	Y

Sample prep & analysis techniques

- Calcite group from crushed Carrara marble

- Both gouges sieved to $<250\mu m$

- 5 g of calcite gouge used to get 3 mm thickness for SHIVA tests

- 15 g of calcite gouge used to get 3mm thickness for Phv tests

- Dark grey dolomite marker is sheared in slip & finite strain fashion @ different positions within gouge layer

- $\tau = \tan \phi = dx/x = $ horizontal displacement/layer thickness

Results

- **Mechanical behavior of room-dry & water-dampened calcite gouge**
  - In SHIVA, peak stress (σ_{peak}) is 2.5-16 MPa @ 3-20 MPa normal stress (σ_n) correlating to peak friction coefficient ($\mu = \tau/\sigma_n$) of ~0.6 to 0.7
  - Absolute shear stress values higher in Phv than in SHIVA
  - Compaction rate change higher for room-dry samples
  - Strengthening phases shorten with increased σ_n in room-dry experiments
  - Higher acceleration, longer strengthening phases for SHIVA tests in wet conditions than for Phv
  - 2 water-dampened SHIVA tests suggest rising length of strengthening values
 - Dynamic weakening initiates after strengthening phase

Results

Table 3

Experimental results. Length of strengthening phase ($d_{strength}$), peak and steady state shear stress (τ_{peak} and τ_{ss}, respectively) with uncertainty ranges (min. and max. values) for a) room-dry and b) wet experiments.

|	Experiment	$d_{strength}$ (m)	$d_{strength,min}$ (m)	$d_{strength,max}$ (m)	τ_{peak} (MPa)	$\tau_{peak,min}$ (MPa)	$\tau_{peak,max}$ (MPa)	τ_{ss} (MPa)	$\tau_{ss,min}$ (MPa)	$\tau_{ss,max}$ (MPa)
a) Room-dry	s897	–	–	–	1.51	1.24	1.77	–	–	–
	s886	0.78	0.48	0.80	2.29	2.15	2.39	1.44	1.20	1.57
	s953	–	–	–	5.14	5.05	5.23	–	–	–
	s871	0.09	0.09	0.10	4.79	4.64	4.93	4.20	3.39	4.32
	s887	0.11	0.08	0.12	5.58	5.17	5.67	–	–	–
	s881	0.09	0.06	0.09	5.27	4.74	5.32	3.06	2.43	3.70
	s1013	0.10	0.10	0.11	5.79	5.61	5.84	3.18	2.90	3.47
	s952	0.19	0.18	0.23	5.64	5.46	5.82	2.63	2.26	3.00
	s896	0.10	0.06	0.11	5.24	4.47	5.42	3.32	2.17	4.47
	s943	0.11	0.11	0.12	5.45	5.24	5.56	2.88	2.37	3.40
	s875	0.08	0.05	0.08	11.27	11.00	11.53	–	–	–
	s889	0.03	0.03	0.04	14.50	14.31	14.68	5.38	4.84	5.91
	phv299	0.13	0.13	0.13	7.79	7.74	7.84	1.79	1.67	2.16
	phv301	0.15	0.14	0.15	7.85	7.77	7.89	1.54	1.12	2.07
	phv311	0.56	0.33	0.58	2.59	2.24	2.60	1.28	1.18	1.39
	phv343[a]	0.29	0.28	0.40	2.79	2.64	2.82	1.57	1.44	1.70
b) Water-dampened/-saturated	s959	0.0055	0.0013	0.0060	4.81	4.47	5.36	–	–	–
	s895	0.0015	0.0010	0.0043	4.62	4.37	4.96	3.69	3.53	3.92
	s961	0.0082	0.0038	0.0530	4.71	4.62	4.85	3.70	3.30	4.15
	s898	0.0030	0.0023	0.0638	4.87	4.53	5.39	3.77	3.32	4.21
	s962	0.0052	0.0014	0.0085	4.75	4.45	5.30	3.86	3.54	4.18
	s279	0.0058	0.0043	0.0074	11.49	10.94	11.69	4.36	3.70	5.02
	s389	0.0423	0.0378	0.0569	11.72	5.38	18.07	4.20	3.14	5.27
	phv291	0.0021	0.0017	0.0023	5.86	5.38	6.34	1.79	1.55	2.03
	phv292	0.0011	0.0006	0.0013	5.29	5.38	5.20	1.34	1.22	1.46
	phv297	0.0011	0.0011	0.0324	5.51	5.38	5.65	1.43	1.14	1.71
	phv298	0.0014	0.0013	0.0507	5.79	5.38	6.20	2.36	2.05	2.67
	phv300	0.0008	0.0006	0.0676	5.78	5.38	6.18	3.00	2.84	3.17
	phv312	0.0009	0.0007	0.0012	5.76	5.38	6.14	1.79	1.55	2.02
	phv306	0.0080	0.0066	0.0574	3.22	5.38	1.06	0.52	0.42	0.61
	phv310	0.0011	0.0009	0.0015	3.94	5.38	2.51	1.14	0.95	1.33
	phv307	0.0008	0.0007	0.0008	6.06	5.38	6.75	2.17	1.95	2.38
	phv309	0.0006	0.0006	0.0008	7.05	5.38	8.72	2.23	1.90	2.56
	phv304	0.0046	0.0035	0.0048	3.90	5.38	2.42	1.11	0.99	1.24
	phv305	0.0136	0.0130	0.0141	3.15	5.38	0.91	0.36	0.29	0.44
	phv340	0.0038	0.0036	0.0040	3.76	5.38	2.14	0.90	0.67	1.24
	phv350	0.0036	0.0036	0.0046	3.92	5.38	2.45	1.41	0.96	1.87
	phv290	0.0077	0.0077	0.0120	3.47	5.38	1.57	0.69	0.65	0.73
	phv337	0.0130	0.0109	0.0154	3.36	5.38	1.35	0.66	0.50	0.83
	phv355	0.0346	0.0047	0.0346	3.29	5.38	1.20	0.28	0.25	0.31
	phv351	0.0139	0.0038	0.0144	3.50	5.38	1.61	0.47	0.42	0.52
	phv313[a]	0.0066	0.0060	0.1754	3.86	5.38	2.34	1.31	1.12	1.50
	phv347[a]	0.0007	0.0006	0.0048	3.22	5.38	1.06	0.13	0.10	0.24

[a] Phv-experiments without pre-shearing.
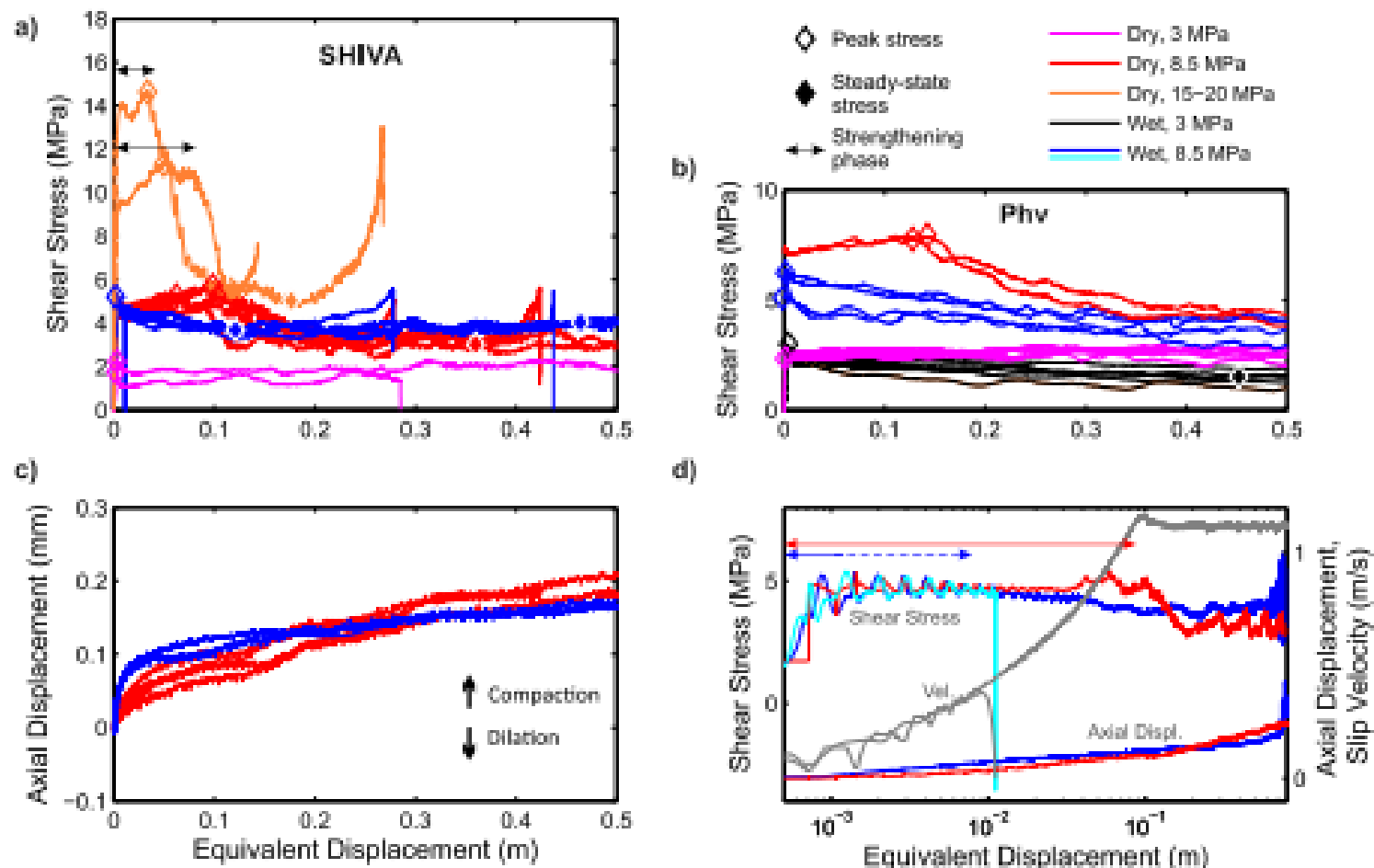
Fig. 3. Mechanical Data. a) Shear stress vs. equivalent displacement for experiments conducted with SHIVA using a target slip rate of 1 m/s and an acceleration of 6 m/s². Color coding corresponds to different ambient conditions and normal stresses used (see legend, valid for all subplots). The strengthening phase, i.e. the slip distance to the onset of dynamic weakening, is indicated with double-headed arrows. A slight misalignment of the axial columns of the apparatus causes oscillations in the shear stress, which are more severe at higher normal stresses. b) Shear stress vs. equivalent displacement for experiments conducted with the Phv apparatus using a target slip rate of 1 m/s and an acceleration of 0.5 m/s². c) Evolution of the axial displacement with equivalent displacement in room-dry (red) and water-dampened (blue) experiments performed with SHIVA. A positive displacement denotes compaction, a negative dilation. d) Evolution of shear stress and axial displacement (secondary y-axis) during the acceleration stage (slip rate is labeled Vel. and plotted in grey also on the secondary y-axis) to better resolve the strengthening phase, which is schematically annotated for both a room-dry (red line) and water-dampened (blue and cyan lines) experiments. The apparent large increase in compaction at the end of the water-dampened experiment is in fact an oscillation likely caused by a misalignment of the axial column; the oscillation can also be observed in the shear stress. (For interpretation of the references to colour in this figure legend, the reader is referred to the web version of this article.)

Results
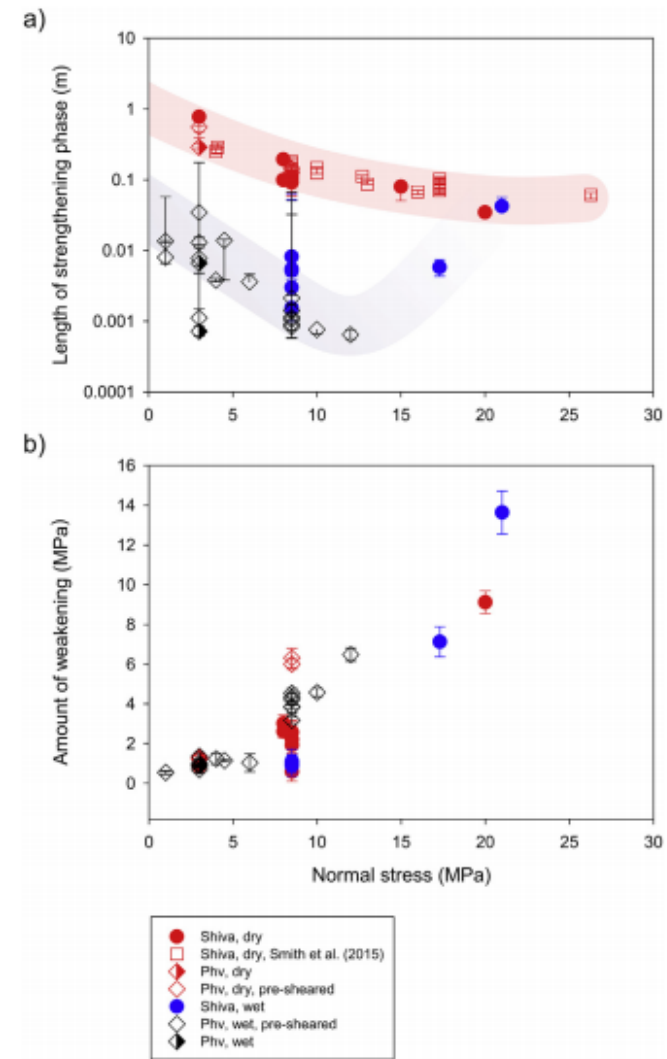
Fig. 4. Dependence of strengthening phase and degree of weakening on the normal stress. a) Length of the strengthening phase (i.e. the slip distance to the onset of dynamic weakening) on a logarithmic scale and b) degree of weakening in room-dry (red symbols) and water-dampened (blue and black symbols) conditions vs. the applied normal stress for experiments performed at a slip velocity of 1 m/s. Filled circles indicate experiments performed with SHIVA, diamonds indicate data from experiments performed with the Phv apparatus, which is equipped with a controlled pore-fluid pressure system. Semi-filled diamonds indicate that the gouge was pre-sheared at 1 mm/s for 30 cm. Squares show data obtained by Smith et al. (2015) using SHIVA. Where no error bars can be seen, the error is smaller than the data points. (For interpretation of the references to colour in this figure legend, the reader is referred to the web version of this article.)

Results

- **Progressive microstructure development**
  - Microstructure of sheared calcite gouge changes w/displacement growth
  - In both wet & dry gouges, zone of comminution grows
  - Both samples show rapid change from high to low strain
  - Little change in preserved samples in microstructure of both dry & wet gouges
  - Both gouges show high strain zone go from general zone of slightly compacted pulverized powder to highly comminuted and compressed gouge sliced by a discrete principal slip surface
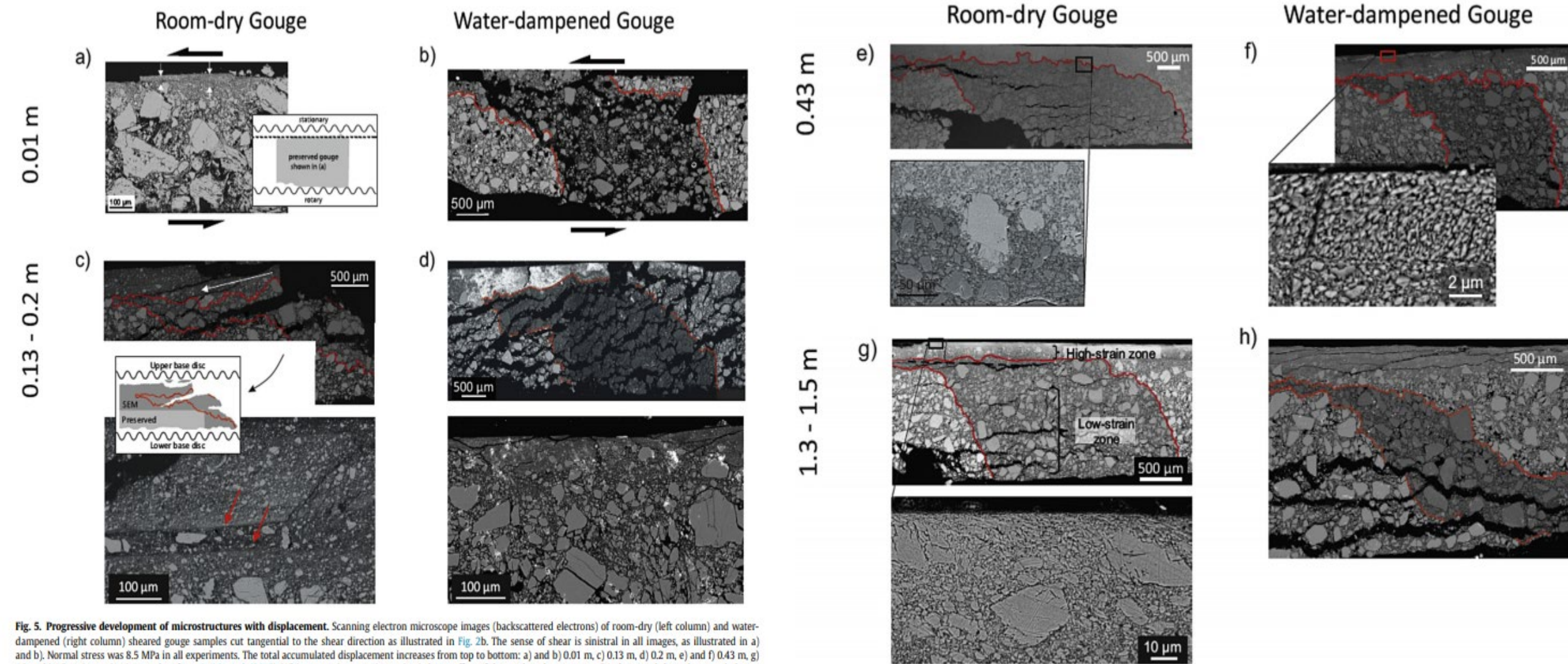
Fig. 5. Progressive development of microstructures with displacement. Scanning electron microscope images (backscattered electrons) of room-dry (left column) and water-dampened (right column) sheared gouge samples cut tangential to the shear direction as illustrated in Fig. 2b. The sense of shear is sinistral in all images, as illustrated in a) and b). Normal stress was 8.5 MPa in all experiments. The total accumulated displacement increases from top to bottom: a) and b) 0.01 m, c) 0.13 m, d) 0.2 m, e) and f) 0.43 m, g) 1.3 m, h) 1.5 m. Image in a) was taken from Smith et al. (2015). White arrow in upper image c) shows offset of the marker along an open R1-shear, and the red arrows in lower image point at several shear bands. White areas in d) are due to sample preparation (Pb from polishing). Lower image in d) is a higher magnification of the high-strain zone. (For interpretation of the references to colour in this figure legend, the reader is referred to the web version of this article.)

Results

- **Quantitative strain analysis**
  - 14 of 18 SHIVA experiments kept a strain marker used to add up strain distribution in gouge layer
  - Marker boundaries appear straight and are traceable
  - Angle of distortion (0-60°) leads to low strains (0-2 Mpa)
  - Finite strain solved by subtracting finite strain from low to intermediate strain zones from bulk strain
  - Finite strain show little to no total displacement dependence, & is similar in dry & wet samples
  - At short total displacements, high strain zone's strain is bigger in water-dampened tests than non-dry tests

Results
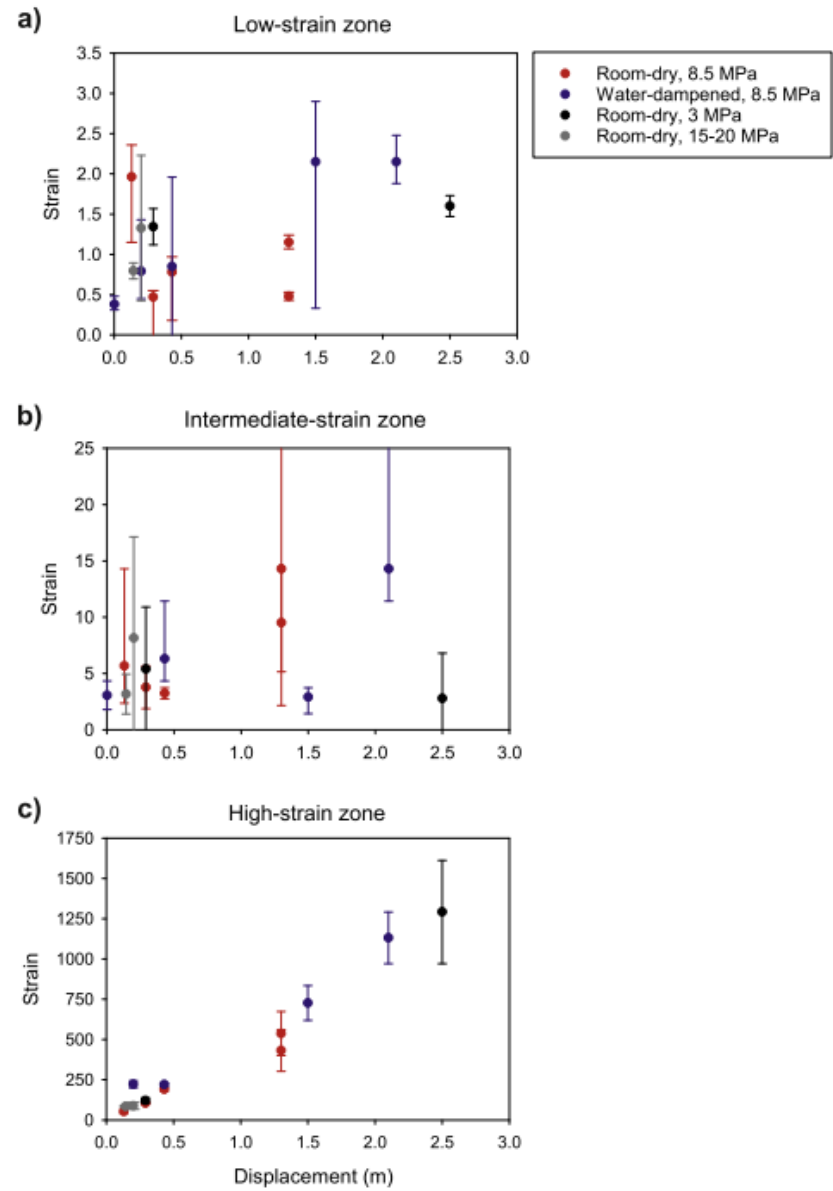
Fig. 6. **Strain distribution in the gouge layer.** Quantitative strain data as obtained from measurement of the angle of distortion of the sheared marker vs. the total equivalent displacement of the respective sample. The strain was determined separately for a) the low-strain zone, b) the intermediate-strain zone and c) the high-strain zone.

Discussion

- **PURPOSE: to investigate water's effect on strain localization process in calcite groups**

- **Progressive strain localization**
  - No microstructural differences
  - Most slip is hosted in principal slip zone after localization is met regardless of conditions suggesting the presence of substantial strain & velocity gradient
  - Calcite gouge tests @ high velocity shows quicker dynamic weakening w/water present
  - Gouges w/20% H_2O (SHIVA) behaved in same way as completely saturated gouges deformed w/stable pore pressure (Phv)
  - Rapid weakening in wet conditions not caused by faster localization
  - Emergence of dynamic weakening in calcite-bearing fault zone relies on normal stress.

Discussion

- **Potential dynamic weakening mechanisms**
  - More efficient or different active weakening mechanism for rapid weakening in wet conditions
  - Phv pore pressure is not elevated, has little effect on mechanical behavior, based on results from SHIVA & Phv
  - High efficiency stress corrosion in wet conditions due to 3x less fracture surface energy for calcite in water
  - Lower steady-state shear stress & higher levels of weakening under dry conditions

Discussion

- **Implications for natural faults**
  - If critical shear stress due to tectonic loading is met, frictional sliding will occur & potential for dynamic weakening of a fault increases
  - Gouge-bearing faults in carbonates become vulnerable to rapid dynamic weakening in water at shallow depths
  - Results say dynamic weakening will come sooner in slip zone water

Conclusion

- Difference in mechanical behavior for wet & dry gouges @ 1 m/s
  - Dry gouges show extended strengthening phase prior to dynamic weakening
  - Wet gouges dynamically weaken instantaneously to a slightly larger steady-state shear stress
- High strain slipping zone & slip surface set up most of displacement
- Amount of strain & velocity gradient found in gouge's thin layer

References

- Ben-Zion, Y., Sammis, C.G., 2003. Characterization of Fault Zones. Pure Appl. Geophys. 160 (3-4), 677-715

- Boullier, A.M., Yeh, E.C., et al., 2009. Microscale anatomy of the 1999 Chi-Chi earthquake fault zone. Geochem. Geophys. Geosyst. 10.

- Bullock, R.J., De Paola, N., et al., 2015. An experimental investigation into the role of phyllosilicate content on earthquake propogation during seismic slip in carbonate faults. J. Geophys. Res. Solid Earth 120 (5), 3187-3207

- Chester, F.M., Chester, J.S., 1998. Ultracataclasite structure and friction processes of the Punchbowl fault, San Andreas system, California. Tectonophysics 295 (1), 199-221

- Chester, F.M., Evans, J.P., et al., 1993. Internal structure and weakening mechanisms of the San-andreas fault. J. Geophys. Res. Solid Earth 98 (B1), 771-786

- De Paola, N., Hirose, T., et al., 2011. Fault lubrication and earthquake propogation in thermally unstable rocks. Geology 39 (1), 35-38.

- Di Toro, G., Niemeijer, A., et al., 2010. From field geology to earthquake simulation: a new state-of-the-art tool to investigate rock friction during the seismic cycle (SHIVA). Rendiconti lincei 21 (1), 95-114.

- Faulkner, D., Mitchell, T., et al., 2011. Stuck in the mud? Earthquake nucleation and propagation through accretionary forearcs. Geophys. Res. Lett. 38 (18).

- Fondreist, M., Smith S.A., et al., 2012. Fault zone structure and seismic slip localization in dolostones, an example from the Southern Alps, Italy. J. Struct. Geol. 45, 52-67.

- Fondreist, M., Smith, S.A.F., et al., 2013. Mirror-like faults and power dissipation during earthquakes. Geology 41 (11). 1175-1178.

- Han, R., Hirose, T., 2012. Clay-clast aggregates in fault gouge: an unequivocal indicatorof seismic faulting at shallow depths? J. Struct. Geol. 43, 92-99
- Han, R., Hirose, T., et al., 2010. Strong velocity weakening and powder lubrication of simulated carbonate faults at seismic slip rates. J. Geophys. Res. Solid Earth 115 (B3).
- Heermance, R., Shipton, Z.K., et al., 2003. Fault structure control on fault slip and ground motion during the 1999 rupture of the Chelungpu fault, Taiwan. Bull. Seismol. Soc. Am. 93 (3). 1034-1050.
- Herwegh, M., Handy, M. 1998. The origin of shape preferred orientations in mylonite: inferences from in-situ experiments on polycrystalline norcamphor. J. Struct. Geol. 20 (6), 681-694.
- Morrow, C., Moore, D.E., et al., 2000. The effect of mineral bond strength and adsorbed water on fault gouge frictional strength. Geophys. Res. Lett. 27 (6), 815-818.
- Proctor, B., Mitchell, T., et al., 2014. Dynamic weakening of serpentinite gouges and bare surfaces at seismic slip rates. J. Geophys. Res. Solid Earth 119 (11), 8107-8131.
- Rockwell, T.K., Ben-Zion, Y., 2007. High localization of primary slip zones in large earthquakes from paleoseismic trenches: observations and implications for earthquake physics. J. Geophys. Res. Solid Earth 112 (B10).
- Sibson, R.H., 2003. "Thickness of the seismic slip zone." Bull. Seismol. Soc. Am. 93 (3), 1169-1178.
- Siman-Tov, S., Aharonov, E., et al., 2013. Nanograins form carbonate fault mirrors. Geology 41 (6), 703-706.
- Smith, S., Nielsen, S., et al., 2015. Strain localization and the onset of dynamic weakening in calcite fault gouge. Earth Planet. Sci. Lett. 413, 25-36.
- Smith, S.A.F., Di Toro, G., et al., 2013. Coseismic recrystallization during shallow earthquake slip. Geology 41 (1), 63-66.
- Snoke, A.W., Tullis, J., et al., 1998., Fault-related rocks: A Photographic Atlas. Princeton University Press.
- Tadai, O., Tanikawa, W., et al., 2009. Design of new frictional testing machine for shallow fault materials. In: AGU Fall Meeting Abstracts.
- Tanikawa, W., Mukoyoshi, H., et al., 2012. Experimental investigation of the influence of slip velocity and temperature on permeability during and after high-velocity fault slip. J. Struct. Geol. 38, 90-101.
- Ujiie, K., Tsutsumi, A., 2010. High-velocity frictional properties of clay-rich fault gouge in a megasplay fault zone, Nankai subduction zone. Geophys. Res. Lett. 37.
- Verbene, B.A., Plumper, O., et al., 2014b. Superplastic nanofibrous slip zones control seismogenic fault friction. Science 346 (6215), 1342-1344.